Accepted Article

Influence of the MJO on daily surface air temperature over Iran

Farnaz Pourasghar[1], Eric C. J. Oliver [2,3], Neil J. Holbrook [1,3]

1. Institute for Marine and Antarctic Studies, University of Tasmania, Hobart, Tasmania, Australia
2. Department of Oceanography, Dalhousie University, Halifax, Nova Scotia, Canada
3. ARC Centre of Excellence for Climate Extremes, University of Tasmania, Hobart, Tasmania, Australia

Corresponding author: Farnaz Pourasghar

Email: **pourasghar.farnaz@gmail.com**

This article has been accepted for publication and undergone full peer review but has not been through the copyediting, typesetting, pagination and proofreading process which may lead to differences between this version and the Version of Record. Please cite this article as doi: 10.1002/joc.7086

This article is protected by copyright. All rights reserved.

Accepted Article

Abstract:

The influence of the Madden-Julian Oscillation (MJO) on surface air temperature over Iran is examined using daily data from meteorological stations from 1979-2015. Composites of daily surface air temperature anomalies are positive in MJO phases 1 and 8 and negative in MJO phases 3-4 with broader region positive tendencies also in MJO phases 2 and 7, and negative tendencies in MJO phases 5-6. This variability is associated with horizontal temperature advection, whereby the southerly (northward) winds act to heat and the northerly (southward) winds cool Iran, in association with the MJO. Further, we find that daily minimum surface air temperatures respond more strongly to the MJO than do daily maximum surface temperatures. These signals correspond to cloudy and humid conditions.

Key words: Madden-Julian Oscillation, surface air temperature, Iran.

This article is protected by copyright. All rights reserved.

Accepted Article

1. Introduction

In recent years, Iran has witnessed a rapid increase in the frequency, severity, duration and geographic extent of extreme weather/climate events (Rahimi and Hejabi, 2017). Key examples of climatic extremes that play important roles in the region are flood, drought and heatwaves which can significantly impact the social and economic activities in Iran (Ahmadnezhad et al., 2013; Keshavarz et al., 2013). However, understanding the linkage between extreme events and large-scale climate variability can be beneficial to the potential predictability of such extremes and can enable longer-term planning.

The Madden-Julian Oscillation (MJO) is the major mode of tropical atmospheric variability on intraseasonal time scales (Madden and Julian, 1971, 1972, 1994; Zhang 2005). The MJO is a large-scale variation in tropical convection with a predominant period of 30-60 days and eastward propagation. It has a significant influence on extratropical atmospheric variability, associated with Rossby wave propagation (e.g. Mathews et al. 2004). It has been shown that the MJO influences tropical cyclones (Bessafi and Wheeler, 2006; Ho et al., 2006), the Asian summer monsoon (Seo et al., 2007; Hoyos and Webster, 2007), North Atlantic Oscillation (Lin et al. 2009), African monsoon (Maloney and Shaman, 2008), and the jet streams (Seo and Son, 2012).

The influence of the MJO on surface air temperature (SAT) has been assessed globally and regionally. Vecchi and Bond (2004) showed that the MJO affects winter SAT at high latitudes in the Northern Hemisphere. Lin and Brunet (2009) found that the MJO significantly influences SAT in southeastern Canada. The MJO also affects wintertime SAT in East Asia and can amplify cold surges from normal to extreme grades (Jeong et al., 2005). Pan and Li (2008) investigated the interaction between MJO and midlatitude low-frequency flow with focus on the effect of the synoptic eddy feedback. The result showed that atmospheric heating associated with the MJO can excite a significant midlatitude response. Oliver (2014) has shown that the relationship between the MJO and SAT over Alaska was significant during the 20th century, although the strength of this relationship varied during different periods of the Pacific Decadal Oscillation. Zhou et al. (2011) showed the relationship between the MJO and Northern Hemisphere SAT by the MJO-excitation of Rossby wave propagation away from the tropics. Zhou et al. (2016) explored the relationship between the MJO and 2m air temperature over central Asia in boreal winter. During MJO phases 3 and 4 (7 and 8), SAT anomalies exhibit a significantly strong negative (positive) response to the MJO from Saudi Arabia to northwestern China. Zhou et al. (2018) analysed the reforecast of 11 models in the subseasonal-to-seasonal (S2S) prediction project to investigate the effects of the MJO on prediction skill of winter SAT over China. All the models tend to have lower SAT prediction skill over the Tibetan Plateau than that over other regions of China. Moreover, the initial state and model resolution have important influences on S2S prediction skill. Generally, most of the S2S models at pentads 3 and 4 tend to have a higher prediction skill with MJO at the initial time than without over China. However, the spatial distribution of prediction skill differences due to the

This article is protected by copyright. All rights reserved.

Accepted Article

MJO are not consistent among the 11 models. Planetary-scale teleconnection patterns excited by the MJO over the Northern Hemisphere is the possible reason for the effect of the MJO on SAT prediction skill. Intraseasonal fluctuations of temperature by the MJO have also been demonstrated for the extratropical Southern Hemisphere (Naumann and Varges, 2010; Alvarez et al., 2016).

Furthermore, some studies have shown that the MJO significantly influences precipitation variations over Iran (Nazemosadat and Ghaedamini, 2010; Hoell et al., (2015); Cannon et al., (2016); Nazemosadat and Shahgholian, 2017). Pourasghar et al. (2015) analysed daily precipitation data in the southern part of Iran and showed that there was a significant relationship with wet conditions in MJO phases 1-2, as they favour moisture advection from western parts of the Indian Ocean into southern Iran. In contrast, dry conditions during MJO phases 3 to 6 were shown to be associated with the advection of drier air from the north. Moreover, Pourasghar et al. (2019) demonstrated that the response of Iran's wet season rainfall to the MJO is also influenced further by large-scale atmospheric variations associated with the Indian Ocean Dipole (IOD) rather than by El Niño – Southern Oscillation. Specifically, they found that the negative (positive) IOD strengthens (suppresses) the MJO rainfall relationship in the wet and dry MJO phases.

Many studies have analysed the spatio-temporal variations of temperature and extremes over Iran (Rahimzadeh et al., 2009; Parak et al., 2015; Soltani et al., 2016; Rahimi and Hejabi, 2017). Despite all of these studies, there has been no comprehensive study of interaseasonal SAT variations over Iran. Hence, the aim of this study is to quantitatively analyse the role of the MJO on large-scale atmospheric circulation anomalies, SAT variations and hot extremes over Iran.

3. Data

3.1 Temperature data

Long records of daily surface air temperatures at 2m above the ground (mean, maximum and minimum) between January 1979 and December 2015 (37 years) for 34 stations (Table 1) have been provided by the Iran Meteorological Organization (IMO) and analysed in this study. Data quality checks were carried out to identify missing values and potentially unrealistic climate records prior to undertaking the full study analysis. Only 0.46 % of the data records of stations comprised of missing values and they were deleted from the records .

3.2 MJO index

The eight phases of the MJO were identified using the real-time multivariate MJO (RMM) index (Wheeler and Hendon 2004). This index is formed by the time series (RMM1 and RMM2) associated with the first two empirical orthogonal functions (EOFs) of combined outgoing long-wave radiation (OLR), and the 850 hPa and 200 hPa zonal winds in the equatorial region (Wheeler and Hendon 2004). The daily Wheeler

This article is protected by copyright. All rights reserved.

Accepted Article

and Hendon (2004) MJO index was provided by Australian Bureau of Meteorology (http://www.bom.gov.au/climate/mjo). The index has two components, phase and amplitude. These components describe MJO activity over the entirety of the tropics together with eastward propagation of the corresponding large-scale anomaly patterns. The intensity of MJO activity is quantified by the RMM amplitude, $(RMM1^2+RMM2^2)^{1/2}$. A strong MJO state is defined when the IHR amplitude is unity or greater.

3.3 Atmospheric variables

Daily mean, maximum, minimum SAT and cloud cover at 2°×1.75° on T62 Gaussian grid (192×94 grid cells globally) and 500 hPa geopotential height, sea level pressure (SLP), horizontal wind and air temperature at 850 hPa at 2.5°×2.5° spatial resolution (144×73 grid cells globally) from the NCEP/NCAR reanalysis (Kalany et al. 1996) have been used to analyse the regional-scale mechanisms of surface air temperature variations over Iran.

4. Methods

In this study, we analysed the relationships between SAT and MJO phase over Iran, together with their association with the large-scale atmospheric circulation. All of these data were de-seasonalised to examine at interannual anomalies relative to the background climatological seasonal cycle. The anomalies were calculated by subtracting the climatology from the daily values, where the daily climatology is defined as the daily long-term mean entire period (1979-2015). Composites of SAT anomalies (mean, maximum, minimum) and other atmospheric variables were constructed during each of the MJO phases for days when the MJO amplitude was ≥ 1. To examine the associated regional-scale atmospheric variations we also calculated MJO composites of the temperature advection, geopotential height, SLP, horizontal wind, air temperature and cloud cover.

From the hydrostatic thermodynamic energy equation (e.g. Holton, 2004, Page 53), we can examine the temperature tendency.

$$\frac{\partial T}{\partial t} = -V \cdot \nabla T + S_p w + \frac{Q}{C_p} \qquad (1)$$

Where the temperature advection is $V \cdot \nabla T = \left(u\frac{\partial T}{\partial x} + v\frac{\partial T}{\partial y} + w\frac{\partial T}{\partial z}\right)$, V is velocity (m/s) with directional elements u, v and w in the zonal (x), meridional (y) and vertical (z) directions, T is temperature (K), C_p is the specific heat of dry air (J Kg^{-1} K^{-1}), Sp is the static stability parameter (K Km^{-1}) and Q is the diabatic heating (J). Diabatic heating is calculated as a residual and the static stability term is approximately constant in the horizontal, so changes in the horizontal distribution of this term are primarily due to vertical velocity changes. The hydrostatic thermodynamic energy equation states that vertical motions are balanced by temperature advection when diabatic heating is small, the static stability parameter is nearly constant in horizontal, and the

This article is protected by copyright. All rights reserved.

Accepted Article

local change in temperature term is small (Hoell et al, 2015). Therefore, we only calculate the temperature advection term.

Statistical significances of the results were tested using a Monte Carlo technique (Wheeler et al., 2009, Zohu et al., 2011, 2016, 2018). We randomly shuffled the MJO index relative to the temperature time series. The composite mean SAT was calculated by randomly shuffling the MJO index during each MJO phase for days when the MJO amplitude is >1. We simulated 1000 randomisations of the MJO phase vector. A confidence interval was built from the many iterations, and if the original result was outside of that interval, it was considered to be statistically significant (at a given significance level). This technique preserves the statistical properties of the MJO such as its autocorrelation and frequency distribution of days across phases. This test assesses if the temperature probability, by MJO phase, is greater or less than expected given random climatic variations. The significance test was carried out at the 5% level.

5. Results

5.1 Climatology of surface air temperature over Iran

More than half of Iran is covered by desert and semi-desert terrains. The Alborz Mountains in the north and the Zagros Mountains in the west are the main topographic features in Iran (Fig 1a). Because of this topographic diversity, the spatial distribution of temperature does not have a regular pattern. Fig 1b shows the temperature climatology over Iran from 1979 to 2015 for 34 stations. It is apparent that Iran's southern region is warmer than northern Iran.

5.2 MJO response of surface air temperature

To examine the relationship between the MJO and air temperature over Iran, composites of anomalies in SAT and various other atmospheric variables were constructed for each of the eight MJO phases. First, we analysed the cold (October to March) and warm (April to September) months for mean, maximum and minimum SAT respectively. The effect of MJO on SAT is stronger and more broadly statistically significant during boreal cold months. Therefore, we restricted our further analysis presented here to cold months only. The data used for the composites were phase 1 (443 days), phase 2 (514 days), phase 3 (581 days), phase 4 (529 days), phase 5 (549 days), phase 6 (607 days), phase 7 (589 days), phase 8 (487 days). Fig 2 shows the SAT anomalies using gridded data and station data as a function of MJO phase. SAT anomalies (gridded and station data) over Iran show systematic variation as the MJO propagates from the Indian Ocean into the western Pacific (phase 1-8). Positive (negative) SAT anomalies correspond to phases 1-2 and 7-8 (phase 3-6). Topography plays an important role in setting the probability distribution of temperature, and stations have different probability distributions in each MJO phase. The significance test results for the

This article is protected by copyright. All rights reserved.

Accepted Article

gridded data were consistent with the SAT significance test. The stations flagged with a star and stippling indicate locations where the values were significant at the 5% level. Warm (positive) SAT anomalies correspond to phases 1 and 8 when the MJO convection centre is located over Africa, the western Indian Ocean and Pacific Ocean. Except sought western part of Iran in phase1, it is significant over the country (phase 1 and 8)

Conversely, cold conditions over Iran corresponded with phases 3-6, especially in phases 3 and 4 when the convective centre is located over the Maritime continent and significant over Iran, except in the northwest in phase 3 and in the northern region in phase 4. The other MJO phases were not significantly related to the SAT anomalies. Composite maps of maximum and minimum SAT show that the amplitude response of the minimum SAT to the MJO is larger than the maximum SAT response (Figs 3 and 4). The greatest influence on the minimum SAT was found to be via cold anomalies during phases 3-5. These signals correspond to cloud-free skies and dry conditions. The variation of mean, maximum and minimum SAT anomalies for the gridded data and station data were found to be consistent.

5.3 Large-scale atmospheric forcing

To examine the large-scale atmospheric variations associated with the MJO, composites of geopotential height, SLP, horizontal wind, air temperature, cloud cover and temperature advection which refers to change in temperature caused by movement of air by the wind were constructed.The geopotential height at 500 hPa as a function of MJO phase is displayed in Fig 5. In MJO phase 1, east, southeast, central and northern Asia are dominated by positive geopotential height anomalies and negative anomalies are centred over the eastern Mediterranean Sea, the northern Red Sea, Arabian Peninsula. As a result, a deep trough is formed over the northern Red Sea and the northern Arabian Peninsula in MJO phase 1 favors northward heat advection and moisture transport from the Arabian Sea into Iran, and which increases the cloud cover. The dominance of warm (cold) southerly (northerly) circulation over Iran during phases 1, 2 (3, 4) is consistent with findings in previous studies (e.g. Zhou et al., 2016). Positive (negative) SLP anomalies are seen over south, southeast and East Asia (the Red Sea and eastern Mediterranean Sea and western Asia) in MJO phase 1 (Fig 6). During phases 2-4, the negative geopotential height and SLP anomalies move eastward and dominate over the study area. Negative geopotential height anomalies correspond to an enhanced cyclonic circulation and are consistent with anomalous T850 temperature advection and horizontal winds. In MJO phases 5 to 8, the atmospheric circulation (due to the geopotential height and SLP) is almost opposite to the circulation in MJO phases 1 to 4. The positive geopotential height and SLP anomalies dominate over the Arabian Peninsula and propagate eastward and then extend northward in phases 6 to 8. The MJO composites of anomalies of the air temperature (T850) and wind at 850 hPa represent the features of the low-level troposphere (Figs 5 and 6). During phase 1, T850 anomalies are positive from Iran to Kazakhstan and

This article is protected by copyright. All rights reserved.

Accepted Article

horizontal wind anomalies show an anticyclonic circulation with its centre in north of India and Pakistan and consistent with warm temperature advection over Iran. In phase 2, positive T850 and wind anomalies move to the east, but they are not strong. In phases 3-6, cold temperature advection dominates over Iran. It was found to be consistent with a negative anomaly of T850. It is strong during phases 3 and 4 when the cyclonic circulation, with its centre over the Arabian Sea, moves eastward in phase 4 over India (Fig 7).

During phases 7 to 8, the T850 anomaly is positive over Iran and the cyclonic circulation is centred over the Arabian Sea, India and the Bay of Bengal. As the SLP, geopotential height and wind patterns showthe advection of warm air over Iran occurs from the Arabian Peninsula, Sudan, and Red Sea, moisture is transported from the Arabian Sea increasing cloud cover over the region (Figs 5-7). All momentum exchanges between the atmosphere and surface take place through the boundary layer. The atmospheric boundary layer (ABL) is the vertical atmospheric layer influenced by land-atmosphere interaction, and the formation and development of the ABL are related to gradients in surface fluxes such as net radiation and sensible heat which lead to mechanical turbulence, convective activity, thermal turbulence and variation in wind direction and speed (Stewart, 1979; Ao et al., 2017; Cushman-Roisin, 2019).

The surface net short wave radiation is affected by cloud cover and surface albedo. Long wave radiation is mainly influenced by cloud cover and low-level troposphere temperature because most of water vapour and greenhouse gases are in the low-level troposphere (Zhou et al., 2016). Fig 8 shows the anomalies of total cloud cover as a function of MJO phase. The positive (negative) anomaly occurs in phases 1-2, 7-8 (3-6). Positive (negative) cloud cover anomalies impact the short- and long-wave radiation which tend to increase (decrease) air temperature at the lower levels.

6. Discussion and conclusions

This study has investigated the relationship between surface air temperature (SAT) over Iran with the intraseasonally-varying MJO. The analysis of composite maps shows that warm (cold) SAT anomalies are observed during MJO phases 1-8 (3-4), with similar albeit non-uniform broader region tendencies in MJO phases 2,7 (5,6). It shows that the changes in occurrence of warm (cold) events are related to eastward propagation of the MJO convective centre from the western Indian Ocean to the western Pacific. The anomalies of low-level air temperature variations (T850) are consistent with SAT anomaly, which is affected by MJO. We also found that the amplitude response of daily minimum SAT to MJO phase is larger than the daily maximum SAT response.

Cloud cover affects net short- and long-wave radiation. The increase (decrease) in cloud cover anomalies suppresses (enhances) short- and long-wave radiation which results in warmer (cooler) minimum surface air temperatures. Atmospheric circulation anomalies propagate eastward with the MJO convective centre propagation. When the convective centre is over the Indian Ocean, Africa and Pacific Ocean (phases

This article is protected by copyright. All rights reserved.

Accepted Article

1-2 and 7-8), there is an increase in the cloud cover and upward motion over Iran and when the convective centre is over the Maritime Continent (phases 3-6) there is a decrease of cloud cover and downward motion over Central Asia and Iran. This is associated with substantial horizontal temperature advection with northward (southward) winds over Iran acting to warm (cool) the air. In phases 3-6, cold air is transported from the north (Siberia) into Iran and decreases the anomalously warm temperature.

This is the first known study to have comprehensively investigated the influences of the MJO on daily surface air temperature over Iran using both station and gridded observations, and by studying the mean, maximum and minimum SAT variations. Using pentad-averaged data during 34years (1979-2012) and a linear regression model without reducing the length of the data record, Zhou et al. (2016) found that surface air temperature does not respond significantly to the MJO over Iran in boreal winter (December-January-February). In the present study using the station and gridded data, and when the MJO amplitude was ≥ 1, we have highlighted the apparent influence of the MJO on surface air temperature during the cold season (October to March), especially minimum surface air temperature over Iran. Our results indicate that statistically significant responses (at the 5% confidence level) occur during the cold season rather than the warm season.

Our results also corroborate previous studies that show that anomalous circulation over southwest Asia during boreal cold season affects air temperature advection (Hoell et al., 2012, 2015). Moreover, these results show the local conditions in which the MJO could be a good predictor of surface air temperature in Iran.

Finally, we note that this analysis is the first step to understanding intraseasonal variations of surface air temperature over Iran, with the potential to improve their predictability which is particularly important for health and agricultural risk management. Numerical modelling studies will be beneficial in order to further explore this potential for utilising the MJO as a predictor of surface air temperature over Iran.

Acknowledgments

Daily temperature data analysed in this article are from the Iran Meteorological Organization. Daily atmospheric reanalysis data analysed here have been provided by the National Centres for Environmental Prediction (NCEP)/National Centre for Atmospheric Research (NCAR) Reanalysis. The historical reconstruction of the MJO index is available on ECJO's personal website: https://ecjoliver.weebly.com/mjo-reconstruction.html. FP acknowledges travel grant funding from the Australian Research Council Centre of Excellence for Climate System Science (ARCCSS). NJH acknowledges funding from the ARC Centre of Excellence for Climate Extremes (Grant CE170100023). We would like to acknowledge the constructive and very valuable comments provided by the anonymous reviewers and the Associate Editor which helped to significantly improve this manuscript.

This article is protected by copyright. All rights reserved.

Accepted Article

References

Ahmadnezhad, E., Holakouie Naieni, K., Ardalan, A., Mahmoudi, M., Yunesian, M., Naddafi, K., & Mesdaghinia, A. R. (2013). Excess mortality during heat wave, Tehran, Iran: An ecological time-series study. *Journal of Research in health science*, 13, 24-31. PMID: 23772013

Alvarez, M. S., C. S. Vera, Kiladis, G. N., & Liebmann, B. (2016). Influence of the Madden Julian Oscillation on precipitation and surface air temperature in South America. *Climate Dynamics*, 46, 245–262. https:/doi.org/ 10.1007/s00382-015-2581-6

Ao, Y., Li, J., Li, Z., Lyu, S., Jiang, C., & Wang, M. (2017) Relation between the atmospheric boundray layer and impact factors under severe thermal conditions. Advances in Meteorology, https://doi.org/10.1155/2017/8352461

Bessafi, M., & Wheeler, M. C. (2006). Modulation of South Indian Ocean tropical cyclones by the Madden–Julian oscillation and convectively coupled equatorial waves. *Monthly Weather Review*, 134, 638–656, https://doi.org/10.1175/MWR3087.1

Cannon, F., L. M. V. Carvalho, C. Jones, A. Hoell, J. Norris, G. Kiladis, and A. A. Tahir (2016), The influence of tropical forcing on extreme winter precipitation in the western Himalaya, *Clim. Dyn.*, https://doi.org/10.1007/s00382-016-3137-0.

Cushman-Roisin B (2019) Environmental Fluid Mechanics. Chapter 12, Atmospheric Boundary Layers. John Wiley & Sons, Inc.

Ho, C. H., Kim, J. H., Jeong, J. H., Kim, H. S., & Chen, D. (2006). Variation of tropical cyclone activity in the South Indian Ocean: El Niño–Southern Oscillation and Madden-Julian Oscillation effects. *Journal Geophysical Research Atmospheres*. 111, D22101. https:// doi.org/10.1029/2006JD007289.

Hoell, A., Barlow, M. & Saini. R. (2012) The Leading Pattern of Intraseasonal and Interannual Indian Ocean Precipitation Variability and Its Relationship with Asian Circulation during the Boreal Cold Season. J. Climate, 25, 7509– 7526, https://doi.org/10.1175/JCLI-D-11-00572.1.

Hoell, A., Shukla, S., Barlow, M., Cannon, F., Kelley, C. & Funk, C. (2015) The Forcing of Monthly Precipitation Variability over Southwest Asia during the Boreal Cold Season. J. Climate, 28, 7038–7056, https://doi.org/10.1175/JCLI-D-14-00757.1.

Hoell, A., Funk, C., & Barlow, M. (2015) The forcing of southwestern Asia teleconnections by low-frequency sea surface temperature variability during boreal winter. *Journal of Climate*, 28, 1511-1526. https://doi:10.1175/JCLI-D-14-00344.1.

Holton, J. R. (2004) An Introduction to Dynamic Meteorology. Elsevier, 535 pp.

This article is protected by copyright. All rights reserved.

Accepted Article

Hoyos, C. D., & Webster, P. J. (2007). The role of intraseasonal variability in the nature of Asian monsoon precipitation. *Journal of Climate*, 20, 4402–4424. https://doi.org/10.1175 /JCLI4252.1.

Kalnay, E., Kanamitsu, M., Kistler, R., Collins, W., ... Joseph, D. (1996). The NCEP/NCAR 40 year reanalysis project. *Bulletin of the American Meteorological Society* 77: 437–471. https://doi.org/10.1175/1520-0477(1996)077<0437: TNYRP>2.0.co;2

Keshavarz, M., Karami, E., & Vanclay F. (2013). The social experience of drought in rural Iran. *Land use policy*, 30, 120-129. https://doi.org/10.1016/j.landusepol.2012.03.003

Lin, H., Brunet, G., & Derome, J. (2009). An observed connection between the North Atlantic Oscillation and the Madden–Julian oscillation. *Journal of Climate*, 22, 364–380. https://doi.org/10.1175/2008JCLI2515.1.

Lin, H., & Brunet, G. (2009). The influence of the Madden-Julian Oscillation on Canadian wintertime surface air temperature. *Monthly Weather Reveiw*, 22, 364–380. https://doi.org/10.1175/2009MWR2831.1

Madden, R. A., & Julian, P. R. (1971). Detection of a 40–50-day oscillation in the zonal wind in the tropical pacific. *Journal of the Atmospheric Science*. 28, 702–708. https://doi.org/10.1175/1520-0469(1971)028<0702:DOADOI>2.0.CO;2

Madden, R. A., & Julian P. R. (1972). Description of global-scale circulation cells in the tropics with a 40–50-day period. *Journal of the Atmospheric Science*, 29, 1109–1123. https://doi.org/10.1175/1520-0469(1972)029<1109:DOGSCC>2.0.CO;2

Madden, R. A., & Julian P. R. (1994). Observations of the 40–50-day tropical oscillation: A review. *Monthly Weather Reveiw*, 112, 814–837. https://doi.org/10.1175/1520-0493(1994)122<0814:OOTDTO>2.0.CO;2

Maloney, E. D., & Shaman, J. (2008). Intraseasonal variability of the West Africa monsoon and Atlantic ITCZ. *Journal of Climate*, 21, 2898–2918. https://doi.org/10.1175/2007JCLI19

992007JCLI1999.1.

Matthews, A. J., B. J. Hoskins, & Masutani, M. (2004). The global response to tropical heating in the Madden-Julian oscillation during the northern winter. *Quarterly Journal of Royl Meteorological Society*, 130, 1991–2011. https://doi.org/10.1256/qj.02.123

Naumann, G., Vargas, W. M. (2010). Joint Diagnostic of surface air temperature in Southern South America and the Madden – Julian Oscillation. *Weather and Forecast*, 25, 1275-1280. https://doi.org/10.1175/2010WAF2222418.1

This article is protected by copyright. All rights reserved.

Accepted Article

Nazemosadat, M. J., Ghaedamini, H. (2010). On the relationships between the Madden- Julian Oscillation and precipitation variability in southern Iran and the Arabian Peninsula: atmospheric circulation analysis. *Journal of Climate*, 23, 887–904. https://doi.org/10.1175/2009JCLI2141.1

Nazemosadat, M. J., Shahgholian, K. (2017). Heavy precipitation in the southwest of Iran: association with the Madden-Julian Oscillation and synoptic scale analysis. *Climate Dynamics*. https://doi.org/10.1007/s00382-016-3496-6.

Oliver, E. C. J. (2014), Multidecadal variations in the modulation of Alaska wintertime air temperature by the Madden–Julian Oscillation, Theor. Appl. Climatol., 121, 1–11.https://doi.org/10.1007/s00704-014-1215-y

Pan, L. L., & Li, T. (2007). Interactions between the tropical ISO and midlatitude low-frequency flow. *Climate Dynamics*. https://doi.org/10.1007/s00382-007-0272-7

Parak, F., Roshani, A., & Jamalib, J. B. (2015). Trends and anomalies in daily climate extremes over Iran during 1961–2010. *Journal of Environmental and Agricultural sciences*. 2, 11. ISSN: 2313-8629

Pourasghar, F., Tozuka, T., Ghaemi, H., Oettli, P., Jahanbakhsh, S., &Yamagata, T. (2015). Influences of the MJO on intraseasonal rainfall variability over southern Iran. *Atmospheric Science Letter*, 16,110–118. https://doi.org/10.1002/asl2.531

Pourasghar, F., Oliver, E. C. J., & Holbrook, N. J. (2019). Modulation of wet-season rainfall over Iran by the MJO, IOD and ENSO. *International Journal of Climatology. https://*doi.org/ 10.1002/joc.6057

Rahimi, M., &Hejabi, S. (2017). Spatial and temporal analysis of trends in extreme temperature indices in Iran over period 1960-2014. *International Journal of Climatol*. 38, 272-282. https://doi.org/10.1002/joc.5175

Rahimzadeh, F., Asgari, A., & Fattahi, E. (2009). Variability of extreme temperature and precipitation in Iran during recent decades. *Internatioanl Journal of Climatology*. 29, 329-343. https://doi.org/10.1002/joc.1739

Seo, K. H., Schemm, J. K. E., Wang, W., & Kumar, A. (2007). The boreal summer intraseasonal oscillation simulated in the NCEP Climate Forecast System (CFS): The effect of sea surface temperature. *Monthly Weather Reveiw*. 135, 1807–1827, doi:10.1175/MWR3369.1Seo, K. H., & Son, S. W. (2012). The global atmospheric circulation re-sponse to tropical diabatic heating associated with the Madden–Julian oscillation during northern winter. *Journal of Atmospheric Science*. 69, 79–96. https://doi.org/10.1175/2011JAS3686.1

Soltani, M., Laux, P., Kunstmann, H., Stan, K., ... Martin M. V (2016) Assessment of climate variations in temperature and precipitation extreme events over Iran. *Theoretical and Applied Climatology*. 126:775-795. https://doi.org/10.1007/s00704-015-1609-5

This article is protected by copyright. All rights reserved.

Accepted Article

Wheeler, M. C., & Hendon, H. (2004). An All- Season Real-Time Multivariate MJO Index: Development of an index for monitoring and prediction. *Monthly Weather Review*, 132, 1917-1932. https://doi.org/10.1175/1520-0493/92004)132<1917: AARMMI>2.0.CO;2

Wheeler, M. C., Hendon, H. H., Cleland, S., Meinke, H., & Donald, A. (2009). Impact of the Madden- Julian Oscillation on Australian rainfall and circulation. *Journal of Climate*, 22, 1482-1498. https://doi.org/10.1175/2008JCLI2595.1

Zhang, C. (2005). Madden-Julian Oscillation. *Reviews of Geophysics*. 43, RG2003. https://doi.org/10.1029/2004RG000158

Zhou, Y., Thompson, K. R., & Lu, Y. (2011). Mapping the relationship between Northern Hemisphere winter surface air temperature and the Madden-Julian Oscillation. *Monthly Weather Review*. 139, 2439–2454. https://doi.org/10.1175/2011MWR3587.1

Zhou, Y., Lu, Y., Yang, B., Jiang, J., Huang, A., Zhao, Y., La, M., & Yang, Q. (2016). On the relationship between the Madden-Julian Oscillation and 2 m air temperature over central Asia in boreal winter. *Journal of Geophysical Research Atmosphere. 121*, 13250-13272. httpd://doi.org/10.1002/2016JD025651

Zhou, Y., Yang, B., Chen, H., Zhang, Y., Huang, A., La, M. (2018) Effects of the Madden-Julian Oscillation on 2-m Air Temperature Prediction over China during Boreal Winter in the S2S Database. Climate Dynamics. https://doi.org/10.1007/s00382

This article is protected by copyright. All rights reserved.

Accepted Article

Figure captions

Fig.1 a) Topographic map of Iran, and b) Surface air temperature climatology for Iran (1979-2015). Circles indicate the location of stations used in this study.

Fig.2 Daily mean surface air temperature (SAT) anomaly for the cold season (October-March) using gridded observations and station observation data (circles) for MJO phases 1-8. The stations flagged with star and stippling indicate locations where the values are significant at the 5% level. (a) phase 1 (443 days), (b) phase 2 (514 days), (c) phase 3 (581 days), (d) phase 4 (529 days), (e) phase 5 (549 days), (f) phase 6 (607 days), (g) phase 7 (589 days), (h) phase 8 (487 days).

Fig.3 Daily maximum SAT anomaly for the cold season (October-March) using gridded data and station data (circles) for MJO phases 1-8. The stations flagged with star and stippling indicate locations where the values are significant at the 5% level. (a) phase 1 (443 days), (b) phase 2 (514 days), (c) phase 3 (581 days), (d) phase 4 (529 days), (e) phase 5 (549 days), (f) phase 6 (607 days), (g) phase 7 (589 days), (h) phase 8 (487 days)**.**

Fig.4 Daily minimum SAT anomaly for the cold season (October-March) using gridded observations and station observation data (circles) for MJO phases 1-8. The stations flagged with star and stippling indicate locations where the values are significant at the 5% level. (a) phase 1 (443 days), (b) phase 2 (514 days), (c) phase 3 (581 days), (d) phase 4 (529 days), (e) phase 5 (549 days), (f) phase 6 (607 days), (g) phase 7 (589 days), (h) phase 8 (487 days)**.**

Fig.5 Composites of 500 hPa gepotential height anomalies for the cold season (October-March) (unit: m). The anomalies of negative (positive) are drown in dash (solid) lines. Anomalies exceeding the 95% confidence level are shaded. Composites of (a) phase 1 (443 days), (b) phase 2 (514 days), (c) phase 3 (581 days), (d) phase 4 (529 days), (e) phase 5 (549 days), (f) phase 6 (607 days), (g) phase 7 (589 days), (h) phase 8 (487 days).

Fig.6 Composites of SLP anomalies for the cold season (October-March) (unit: hPa). The anomalies of negative (positive) are drown in dash (solid) lines. SLP anomalies exceeding the 95% confidence level are shaded.(a) phase 1 (443 days), (b) phase 2 (514 days), (c) phase 3 (581 days), (d) phase 4 (529 days), (e) phase 5 (549 days), (f) phase 6 (607 days), (g) phase 7 (589 days), (h) phase 8 (487 days).

Fig.7 Composites of air temperature advection anomalies at 850 hPa (contour intervals are 1.0×10^{-5}, unit: K/s) ,wind anomalies, vectors are plotted only where they are statistically significant at the 5% level (vector, unit: ms^{-1}) and air temperature anomalies at 850 hPa (shading, unit: K) with the MJO.

Fig.8 Composites of total cloud cover (in %) for the cold season (October-March). (a) phase 1 (443 days), (b) phase 2 (514 days), (c) phase 3 (581 days), (d) phase 4 (529 days), (e) phase 5 (549 days), (f) phase 6 (607 days), (g) phase 7 (589 days), (h) phase 8 (487 days).

This article is protected by copyright. All rights reserved.

Accepted Article

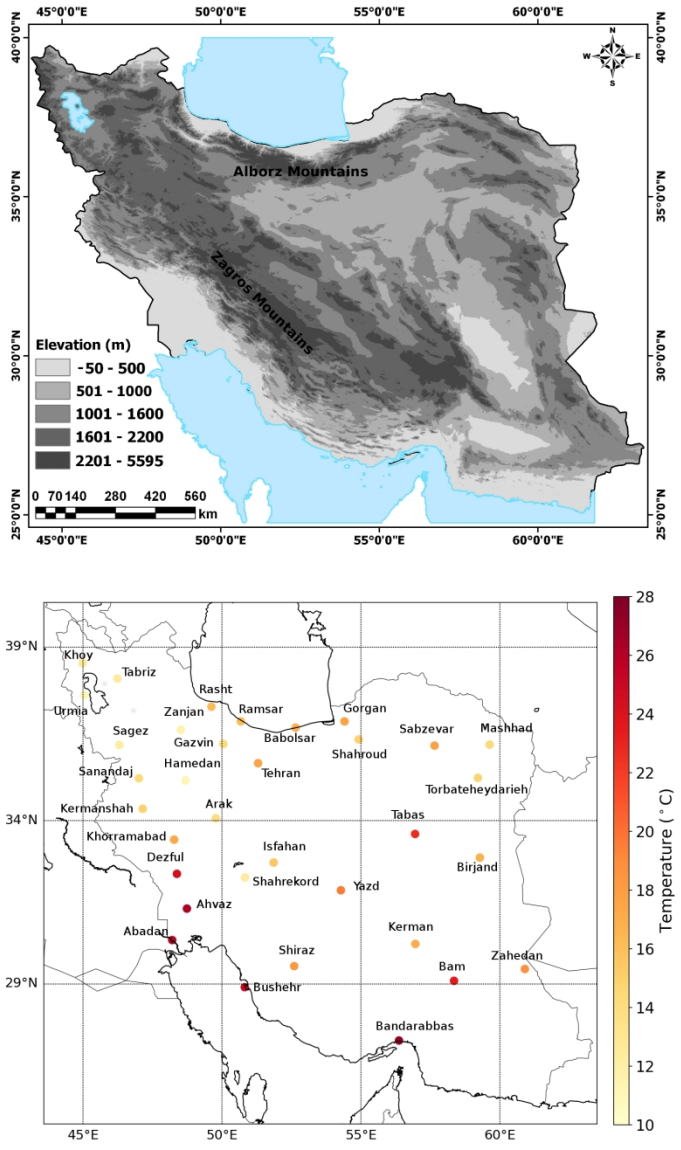

Fig.1 a) Topographic map of Iran, and b) Surface air temperature climatology for Iran (1979-2015). Circles indicate the location of stations used in this study.

This article is protected by copyright. All rights reserved.

Accepted Article

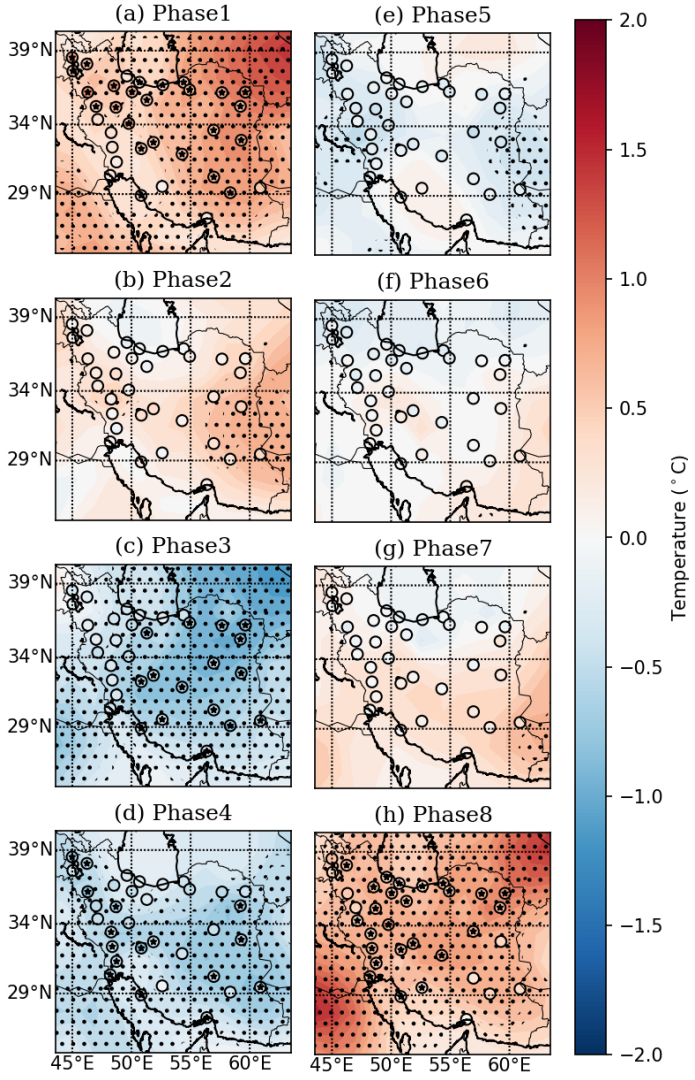

Fig.2 Daily mean surface air temperature (SAT) anomaly for the cold season (October-March) using gridded observations and station observation data (circles) for MJO phases 1-8. The stations flagged with star and stippling indicate locations where the values are significant at the 5% level. (a) phase 1 (443 days), (b) phase 2 (514 days), (c) phase 3 (581 days), (d) phase 4 (529 days), (e) phase 5 (549 days), (f) phase 6 (607 days), (g) phase 7 (589 days), (h) phase 8 (487 days).

169x229mm (150 x 150 DPI)

This article is protected by copyright. All rights reserved.

Accepted Article

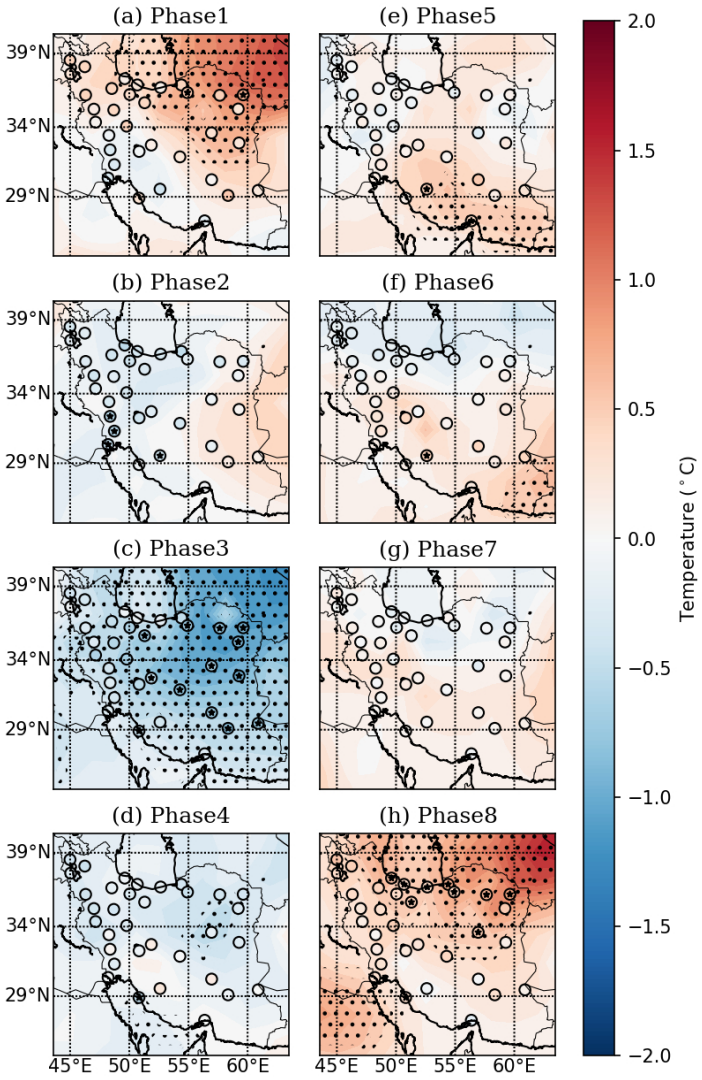

Fig.3 Daily maximum SAT anomaly for the cold season (October-March) using gridded data and station data (circles) for MJO phases 1-8. The stations flagged with star and stippling indicate locations where the values are significant at the 5% level. (a) phase 1 (443 days), (b) phase 2 (514 days), (c) phase 3 (581 days), (d) phase 4 (529 days), (e) phase 5 (549 days), (f) phase 6 (607 days), (g) phase 7 (589 days), (h) phase 8 (487 days).

169x229mm (150 x 150 DPI)

This article is protected by copyright. All rights reserved.

Accepted Article

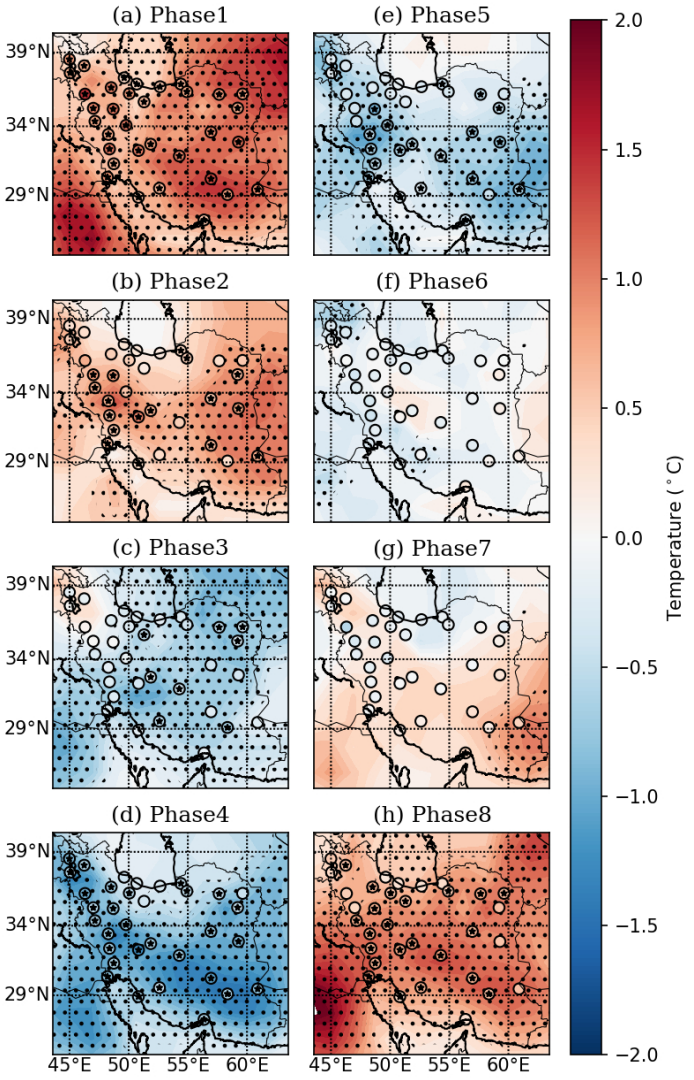

Fig.4 Daily minimum SAT anomaly for the cold season (October-March) using gridded observations and station observation data (circles) for MJO phases 1-8. The stations flagged with star and stippling indicate locations where the values are significant at the 5% level. (a) phase 1 (443 days), (b) phase 2 (514 days), (c) phase 3 (581 days), (d) phase 4 (529 days), (e) phase 5 (549 days), (f) phase 6 (607 days), (g) phase 7 (589 days), (h) phase 8 (487 days).

169x229mm (150 x 150 DPI)

This article is protected by copyright. All rights reserved.

Accepted Article

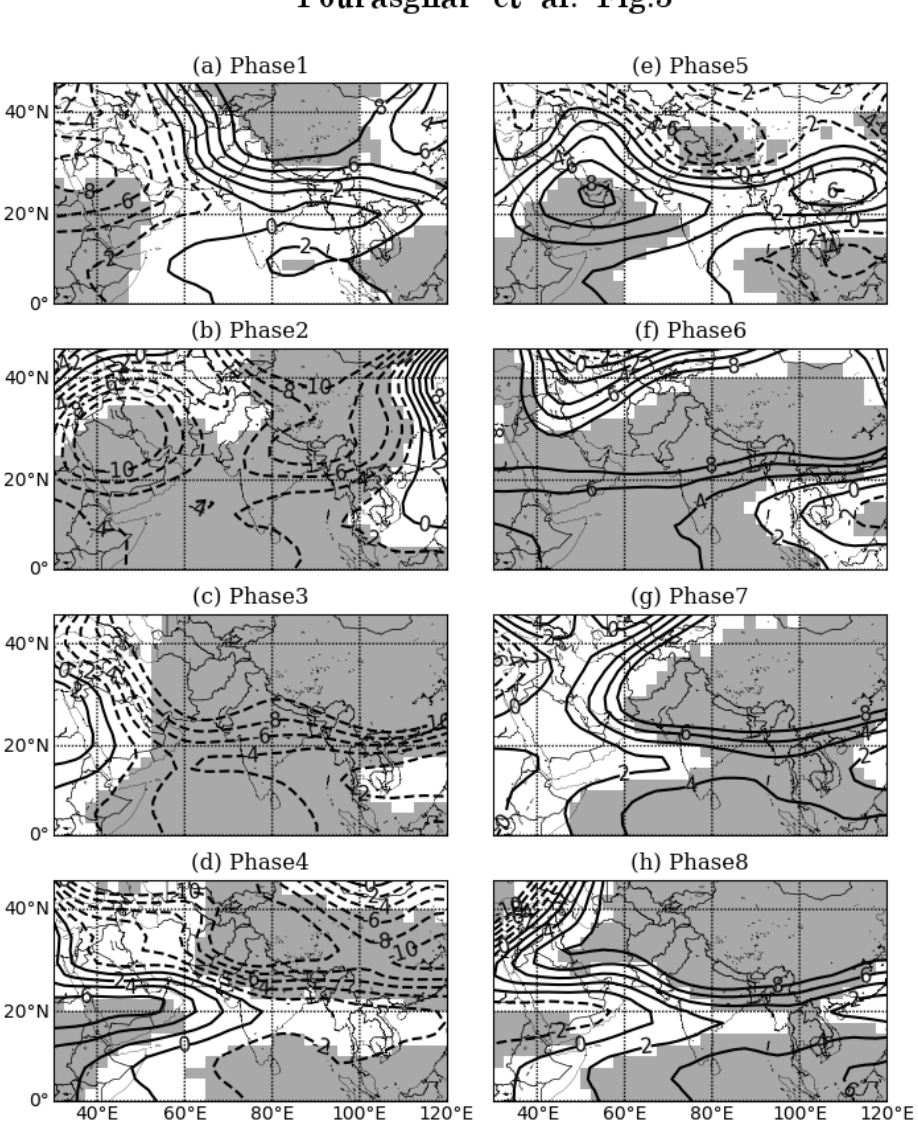

Fig.5 Composites of 500 hPa gepotential height anomalies for the cold season (October-March) (unit: m). The anomalies of negative (positive) are drown in dash (solid) lines. Anomalies exceeding the 95% confidence level are shaded. Composites of (a) phase 1 (443 days), (b) phase 2 (514 days), (c) phase 3 (581 days), (d) phase 4 (529 days), (e) phase 5 (549 days), (f) phase 6 (607 days), (g) phase 7 (589 days), (h) phase 8 (487 days).

190x230mm (100 x 100 DPI)

This article is protected by copyright. All rights reserved.

Accepted Article

Pourasghar et al. Fig. 6

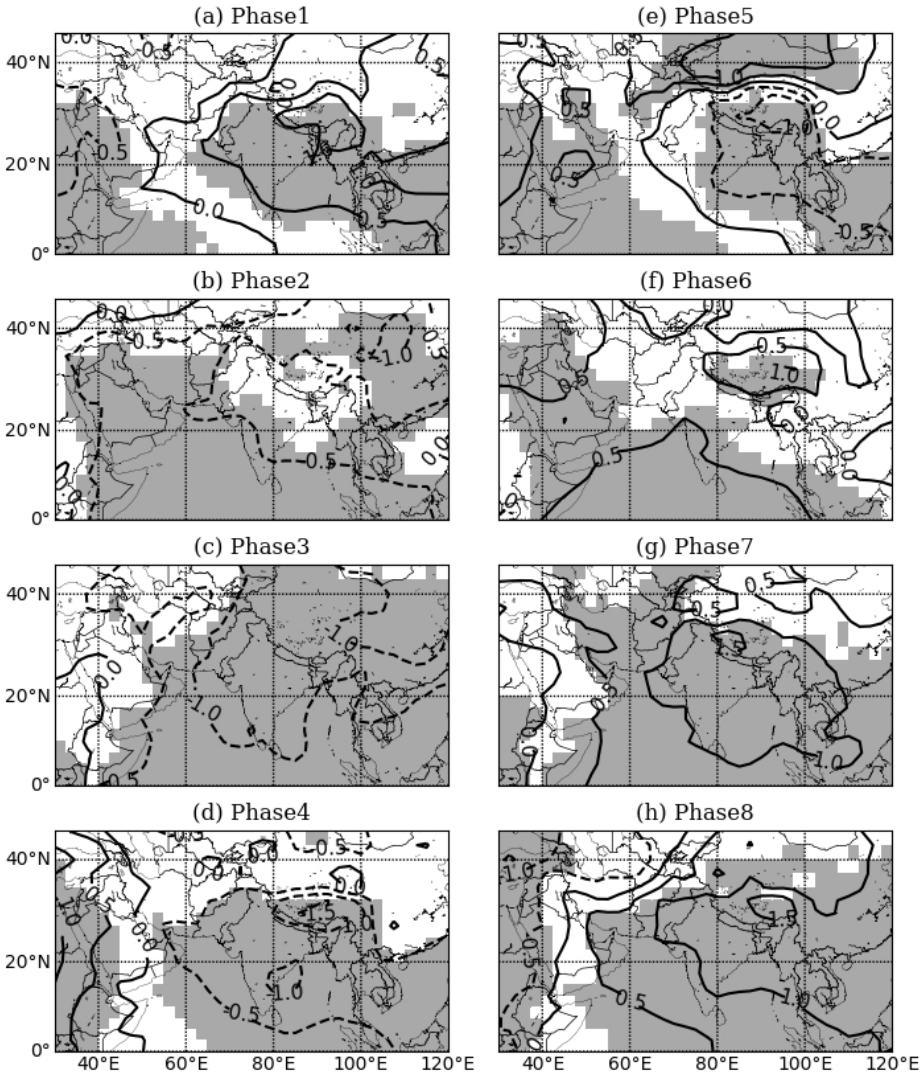

Fig.6 Composites of SLP anomalies for the cold season (October-March) (unit: hPa). The anomalies of negative (positive) are drown in dash (solid) lines. SLP anomalies exceeding the 95% confidence level are shaded.(a) phase 1 (443 days), (b) phase 2 (514 days), (c) phase 3 (581 days), (d) phase 4 (529 days), (e) phase 5 (549 days), (f) phase 6 (607 days), (g) phase 7 (589 days), (h) phase 8 (487 days).

190x230mm (100 x 100 DPI)

This article is protected by copyright. All rights reserved.

Accepted Article

Pourasghar et al. Fig. 7

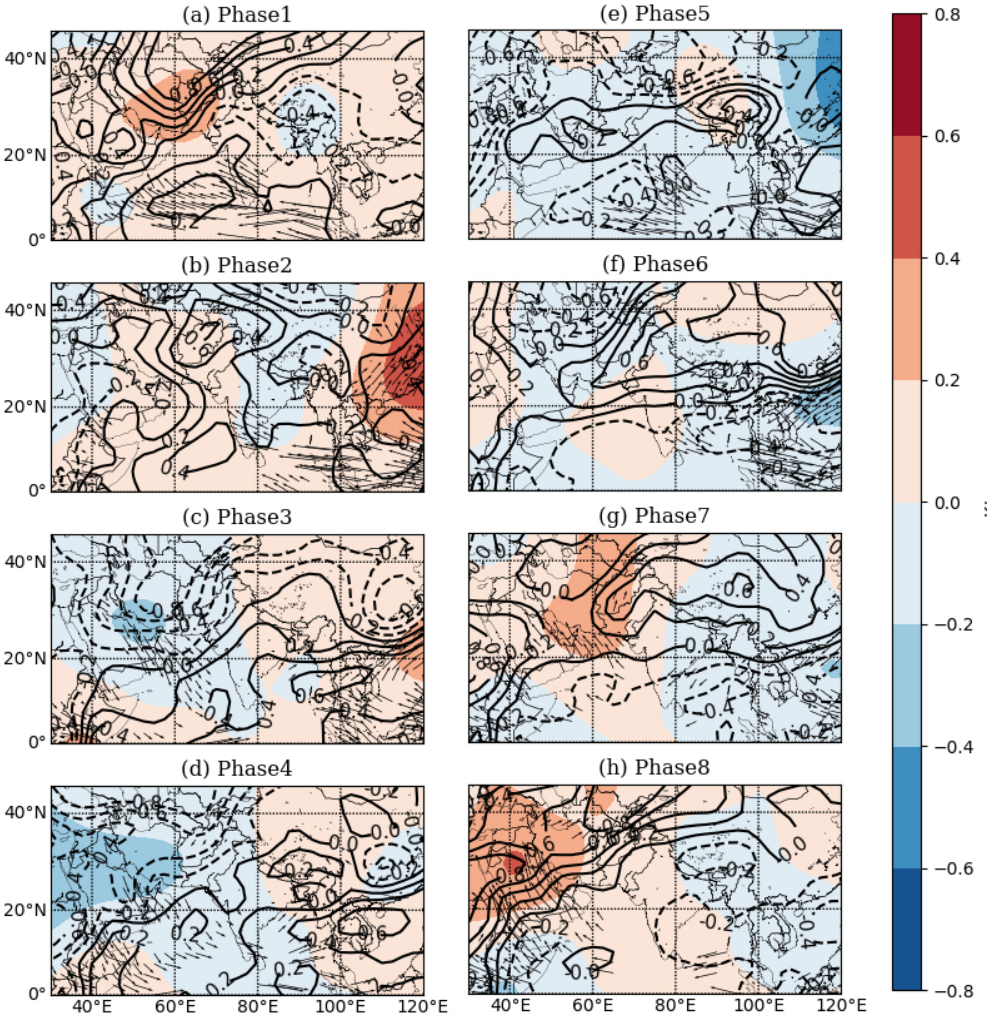

Fig. 7 Composites of air temperature advection anomalies at 850 hPa (contour intervals are 1.0 x 10-5, unit: K/s) ,wind anomalies, vectors are plotted only where they are statistically significant at the 5% level (vector, unit: ms-1) and air temperature anomalies at 850 hPa (shading, unit: K) with the MJO.

203x230mm (100 x 100 DPI)

This article is protected by copyright. All rights reserved.

Accepted Article

Pourasghar et al. Fig.8

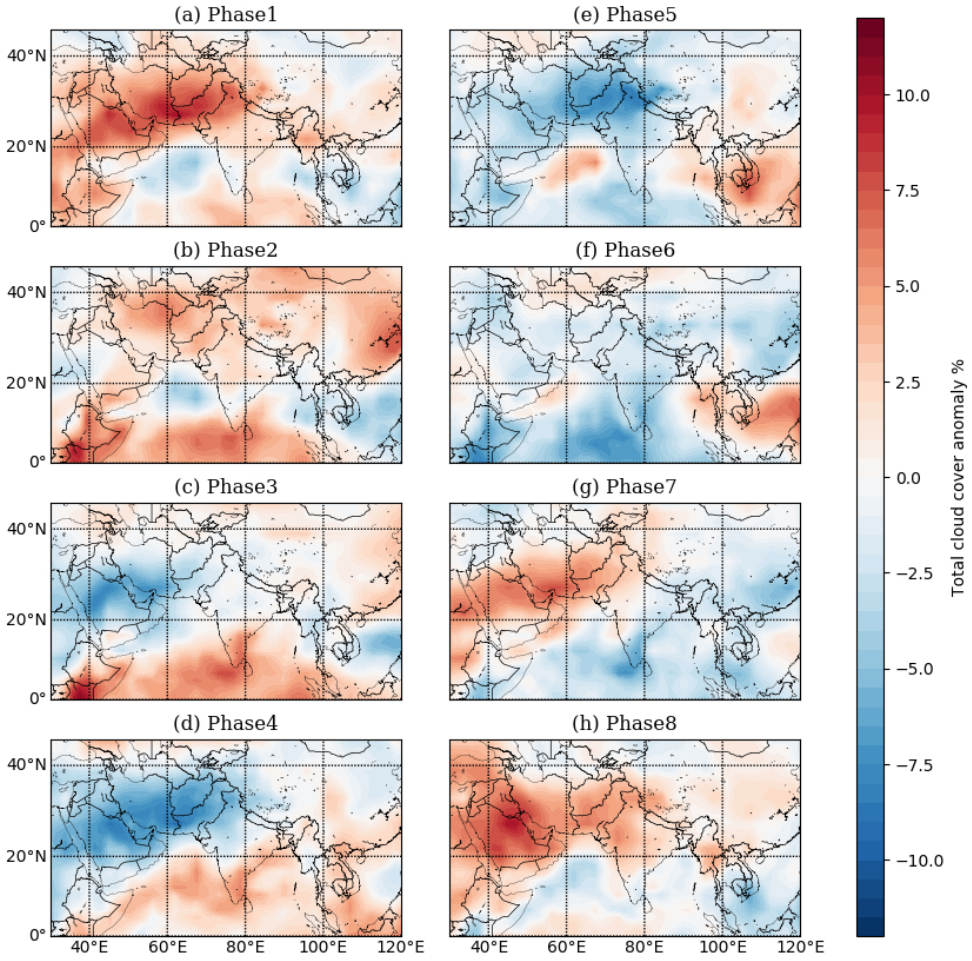

Fig.8 Composites of total cloud cover (in %) for the cold season (October-March). (a) phase 1 (443 days), (b) phase 2 (514 days), (c) phase 3 (581 days), (d) phase 4 (529 days), (e) phase 5 (549 days), (f) phase 6 (607 days), (g) phase 7 (589 days), (h) phase 8 (487 days).

215x230mm (100 x 100 DPI)

This article is protected by copyright. All rights reserved.

Accepted Article

Table Caption

Table. 1 Synoptic meteorological stations and their geophysical characteristics

Station name	Latitude (N)	Longitude (E)	Elevation (m a.s.l.)
Abadan	30.37	48.21	6.6
Ahvaz	31.34	48.74	22.5
Arak	34.07	49.78	1702.8
Babolsar	36.72	52.65	-21
Bam	29.10	58.35	1066.9
Bandarabbas	27.21	56.37	9.8
Birjand	32.89	59.28	1491
Bushehr	28.96	50.81	9
Dezful	32.40	48.38	143
Isfahan	32.74	51.86	1551.9
Gazvin	36.25	50.05	1279.1
Gorgan	36.90	54.41	0
Hamedan	34.86	48.53	1740.8
Kerman	30.25	56.96	1754
Kermanshah	34.35	47.15	1318.5
Khorramabad	33.43	48.28	1147.8
Khoy	38.55	44.99	1103.4
Mashhad	36.23	59.63	999.2
Ramsar	36.90	50.68	-20
Rasht	37.32	49.62	-8.6
Sabzevar	36.20	57.65	972
Sagez	36.22	46.31	1522.8
Sanandaj	35.25	47.01	1373.4
Shahrekord	32.29	50.83	2048.9
Shahrud	36.38	54.92	1325.2
Shiraz	29.56	52.60	1488
Tabas	33.60	56.95	711
Tabriz	38.12	46.24	1361
Tehran	35.69	51.30	1191
Torbateheydariyeh	35.26	59.21	1451
Urmia	37.65	45.05	1328
Yazd	31.90	54.28	1230.2

This article is protected by copyright. All rights reserved.

Zahedan	29.47	60.90	1370
Zanjan	36.77	48.37	1640.7

Accepted Article

This article is protected by copyright. All rights reserved.